Thermally compensated aluminum nitride Lamb wave resonators for high temperature applications

Chih-Ming Lin,[1,2,a)] Ting-Ta Yen,[1,2] Valery V. Felmetsger,[3] Matthew A. Hopcroft,[2,4] Jan H. Kuypers,[2] and Albert P. Pisano[1,2]
[1]*Department of Mechanical Engineering, University of California, Berkeley, California 94720, USA*
[2]*Berkeley Sensor and Actuator Center, University of California, Berkeley, California 94720, USA*
[3]*OEM Group Incorporated, Gilbert, Arizona 85233, USA*
[4]*Hewlett-Packard Labs, Palo Alto, California 94304, USA*

(Received 1 July 2010; accepted 29 July 2010; published online 23 August 2010)

In this letter, temperature compensation for aluminum nitride (AlN) Lamb wave resonators operating at high temperature is presented. By adding a compensating layer of silicon dioxide (SiO_2), the turnover temperature can be designed for high temperature operation by varying the normalized AlN film thickness (h_{AlN}/λ) and the normalized SiO_2 film thickness (h_{SiO_2}/λ). With different designs of h_{AlN}/λ and h_{SiO_2}/λ, the Lamb wave resonators were well temperature-compensated at 214 °C, 430 °C, and 542 °C, respectively. The experimental results demonstrate that the thermally compensated AlN Lamb wave resonators are promising for frequency control and sensing applications at high temperature. © *2010 American Institute of Physics*. [doi:10.1063/1.3481361]

Piezoelectric microelectromechanical system (MEMS) devices capable of operating in high temperature environments have attracted great interest in various industries, including automotive, aerospace, gas and petroleum exploration, and power electronics. Although quartz is the most widely used piezoelectric material because of its chemical inertness and excellent thermal stability at room temperature, the application of quartz at high temperature is limited by the phase transition from trigonal α-quartz to hexagonal β-quartz at 573 °C, which causes discontinuities in its material properties and typically restricts the use of quartz to temperatures below 350 °C.[1] The common candidates of piezoelectric materials for high temperature applications are gallium orthophosphate ($GaPO_4$), langasite, langatate (LGT), and aluminum nitride (AlN).[1–3]

In addition to operating at high temperature, maintaining the temperature stability of the resonance frequency (f_s) in high temperature environments is essential for high temperature applications. For piezoelectric single-crystal materials, different crystal cuts and wave propagation directions can be used to obtain temperature-compensated acoustic devices at different temperatures.[3,4] Recently, Davulis and Pereira da Cunha demonstrated that surface acoustic wave (SAW) devices on LGT can be thermally compensated at different temperatures by varying the SAW propagation directions.[3] For piezoelectric thin film materials, AlN is the most interesting candidate for high temperature applications because it can maintain its piezoelectric properties up to 1150 °C. In addition, AlN thin films do not exhibit phase transitions on heating from room temperature up to the melting point which exceeds 2000 °C in a nitrogen atmosphere.[1] Multiple research efforts are ongoing to demonstrate AlN-based piezoelectric sensors[5] and resonators[6] for high temperature applications. However, the challenge to achieve good frequency-temperature stability at high temperature requires the temperature compensation of AlN thin films.

As is well-known, silicon dioxide (SiO_2) possesses the rare characteristic of the positive first-order temperature coefficients of elasticity (TCE). The thermal compensation technique using a compensating layer of SiO_2 to a device structure has been applied to many different kinds of resonators.[7–13] This present work demonstrates the thermal compensation for AlN Lamb wave resonators operating at high temperature using an AlN/SiO_2 composite structure. By designing composite structures with different normalized AlN thickness (h_{AlN}/λ) and normalized SiO_2 thickness (h_{SiO_2}/λ), Lamb wave resonators with a zero first-order temperature coefficient of frequency (TCF) at 214 °C, 430 °C, and 542 °C are experimentally demonstrated. These thermally compensated Lamb wave resonators exhibit a strong quadratic frequency-temperature behavior with a turnover temperature (T_o).

The thermally stable Lamb wave resonators described in this work are illustrated in Fig. 1(a). The Lamb wave resonator consists of an interdigital transducer (IDT) and a met-

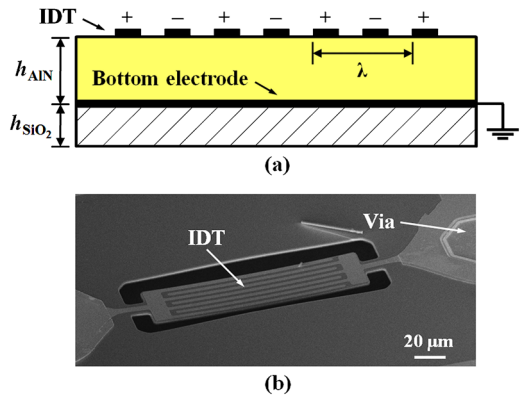

FIG. 1. (Color online) (a) Illustration of the cross-section of the thermally compensated Lamb wave resonator using IDT electrodes with a metalized (short-circuited) surface at the interface of the AlN/SiO_2 composite stack. (b) SEM image of the thermally compensated Lamb wave resonator (design 3) on the AlN/SiO_2 composite stack. The electrical contact via through the AlN layer is used to ground the Pt bottom electrode.

[a)]Author to whom correspondence should be addressed. Electronic mail: gimmylin@berkeley.edu.

alized (short-circuited) surface at the interface of the AlN/SiO_2 composite membranes. The metalized interface significantly enhances the electromechanical coupling coefficient because a strong electric field can be induced between the IDT electrodes and the metalized interface.[11–14] Aluminum (Al) is often used as the electrode material for the bottom electrode and the IDT. However, the Lamb wave resonators are designed to operate at high temperature up to 700 °C so Al is not preferred due to its low melting point of 660 °C. In this study, platinum (Pt) with a melting point at 1768 °C was used as the metallization for the bottom electrode and the IDT. Figure 1(b) shows the scanning electron microscope (SEM) image of the fabricated Lamb wave resonator.

The dispersive characteristics of Lamb waves in the AlN/SiO_2 composite structure are studied by using Alder's approach.[15] The (002) plane of the AlN thin film is parallel to the SiO_2 surface and Lamb waves propagate in the plane normal to the *c*-axis of the AlN thin film. For this case, the first-order TCF of the Lamb wave resonator on the AlN/SiO_2 composite membranes can be theoretically calculated using

$$\mathrm{TCF}_{\mathrm{LWR}} = \frac{1}{v}\frac{\partial v}{\partial T} - \alpha_{\mathrm{eff}}, \tag{1}$$

where v is the Lamb wave phase velocity in the composite stack, T is temperature, and α_{eff} corresponds to the effective thermal expansion coefficient along Lamb wave propagation direction. The effective thermal expansion for an arbitrary stack of layers can be expressed as

$$\alpha_{\mathrm{eff}} = \frac{\Sigma_{i=1}^{n} E_i t_i \alpha_i}{\Sigma_{i=1}^{n} E_i t_i}, \tag{2}$$

where E_i is the Young's modulus of *i*th layer, t_i is the thickness of *i*th layer, and α_i is the thermal expansion coefficient of *i*th layer, respectively.

In the theoretical calculation, the Pt bottom electrode thickness is neglected because the first-order TCE of Pt is not available in literature. The effect of the film stresses is also neglected, and the first-order TCF of the Lamb wave resonator is computed on the basis of the first-order temperature-dependent material properties of AlN and SiO_2 given in literature.[8] The room temperature first-order TCFs of Lamb wave resonators utilizing the lowest symmetric (S_0) mode

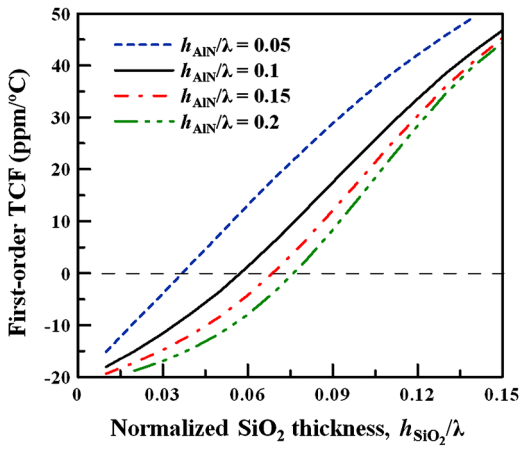

FIG. 2. (Color online) The dispersive characteristics of the room temperature first-order TCF of Lamb wave resonators utilizing the lowest symmetric (S_0) mode in the AlN/SiO_2 composite stack with a metalized interface.

TABLE I. Geometric dimensions of Lamb wave resonators.

	Design 1	Design 2	Design 3	Design 4
Number of IDT electrode	13	13	7	13
IDT aperture (μm)	125	125	100	125
IDT electrode width (μm)	2.77	2.77	2.77	2.21
Metallization ratio	0.5	0.5	0.5	0.5
Pt IDT electrode thickness (nm)	100	100	100	100
Pt bottom electrode thickness (nm)	100	100	100	100
AlN layer thickness (μm)	1.5	1	1	1
SiO_2 layer thickness (μm)	···	1	1.26	1.26

with different h_{AlN}/λ of 0.05, 0.1, 0.15, and 0.2 values are depicted in Fig. 2. In general, the goal is to achieve a zero first-order TCF at room temperature. However, if the Lamb wave resonator is designed to be thermally stable at high temperature, the first-order TCF has to be positive at room temperature. This concept is very similar to SAW devices on LGT for high temperature applications[3] or SC-cut quartz resonators.[4] Therefore, a positive first-order TCF is expected at room temperature because the turnover temperature of the Lamb wave resonator is intended to be at high temperature.

Four different designs of Lamb wave resonators were compared in this work with their geometric dimensions given in Table I. Design 1 resonator has no SiO_2 film beneath the AlN layer and therefore is uncompensated. Design 2 and 3 resonators are designed with the same AlN thicknesses but different SiO_2 thicknesses for comparison. Design 4 resonator has the narrowest IDT electrode width and pitch (i.e., wavelength) among all the designs. In order to determine the frequency-temperature characteristic, Lamb wave resonators were measured in the temperature range from 25 to 700 °C. The temperature was varied in 20 °C steps with 5 min of temperature stabilization time before each measurement.

Figure 3 shows the plot of measured fractional frequency variation versus temperature for the four designed resonators. As expected, design 1 resonator exhibits a large fractional frequency variation which shows an approximate linear function of temperature. In contrast to design 1 resonator, the other three Lamb wave resonators exhibit turnover temperatures at 214 °C, 430 °C, and 542 °C, respectively, at which

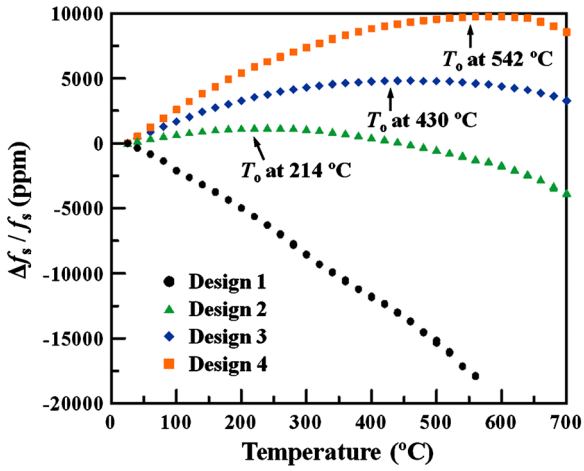

FIG. 3. (Color online) Plot of the measured fractional frequency variation vs temperature of four Lamb wave resonators. Design 1 is an uncompensated resonator, whereas designs 2, 3, and 4 are well temperature-compensated resonators at 214 °C, 430 °C, and 542 °C, respectively.

TABLE II. Comparison of simulated and measured TCF.

	Design 1	Design 2	Design 3	Design 4
Normalized AlN thickness (h_{AlN}/λ)	0.135	0.09	0.09	0.113
Normalized SiO_2 thickness (h_{SiO_2}/λ)	0	0.09	0.114	0.143
Simulated first-order TCF (ppm/°C)	−21.1	18.95	31.7	43.38
Measured first-order TCF (ppm/°C)	−28.14	9.63	22.19	35.73
Measured second-order TCF (ppb/°C^2)	−9.62	−22.58	−25.81	−32.98
Turnover temperature (T_o) (°C)	···	214	430	542

f_s is very insensitive to the temperature changes. The fractional frequency variation in these three temperature-compensated Lamb wave resonators shows a strong quadratic function of temperature. Table II compares the simulated and measured first-order TCF of the four designed resonators. All of the experimental first-order TCF are smaller than the predicted values. The mismatch is likely due to the neglect of the bottom electrode and IDT as well as the neglect of the film stresses in the calculation.[13] In addition, the accuracy of the first-order TCF prediction relies heavily on the accuracy of the material property data. However, the material data at high temperature might differ considerably from the data at room temperature.[3]

Moreover, it should be noted that the second-order TCF becomes more pronounced for a thicker SiO_2 layer. The experimental data and other reported results[16] suggest that the second-order TCE of SiO_2 is negative even though the first-order TCE is positive. In addition, it is clear that the turnover temperature depends heavily on the first-order and second-order TCE data of the materials used in the composite plates. Therefore, it is difficult to predict the precise position of the turnover temperature because reliable TCE constants for AlN, Pt, and SiO_2 are not available in literature. Once reliable TCE data are available, the location of the turnover temperature of the Lamb wave resonator on the AlN/SiO_2 composite membranes can be accurately predicted.

On the other hand, because the Lamb wave resonators were wire-bonded to a printed circuit board for high temperature measurement, the parasitic bonding wire inductance and board pad capacitance degraded the resonator performance. The quality factor (Q), effective coupling coefficient (k_t^2), and motional resistance (R_m) were reduced due to the gold wire bonding. In this study, Q was extracted by using the phase slope method[17] and it is defined as

$$Q = \frac{\omega_0}{2}\left|\frac{d\Phi}{d\omega}\right|, \tag{3}$$

where ω_0 is the angular frequency at resonance and $d\Phi/d\omega$ denotes the slope of the phase of the transfer function with respect to angular frequency. The detailed performance of the Lamb wave resonators after gold wire bonding at room temperature and turnover temperature are summarized in Table III. The experimental results show that the Q was degraded and the k_t^2 increased at high temperature. Material softening and thermoelastic damping are possible reasons for the decrease in Q. The piezoelectric coefficients of AlN thin films increase with temperature,[18] explaining the larger k_t^2 measured at high temperature.

Temperature-compensated Lamb wave resonators operating at high temperature using the AlN/SiO_2 multilayered membranes have been designed, fabricated, and characterized in this study. In order for the resonators to operate at high temperature up to 700 °C, Pt was used as the metal material for the electrodes. Using different normalized AlN and SiO_2 layer thicknesses, complete thermal compensation for the Lamb wave resonators was achieved at 214 °C, 430 °C, and 542 °C, respectively. The results demonstrate the potential of the temperature-compensated Lamb wave resonators on the AlN/SiO_2 composite structure for frequency control and sensing applications at high temperature.

TABLE III. Performance of Lamb wave resonators after gold wire bonding at room temperature and turnover temperature.

	Design 1	Design 2	Design 3	Design 4
f_s at 25 °C (MHz)	861.6	710.3	677.7	835.0
Q at 25 °C	423	665	373	448
Q around T_o	···	391	198	93
k_t^2 at 25 °C (%)	0.31	0.23	0.21	0.23
k_t^2 around T_o (%)	···	0.28	0.31	0.45
R_m at 25 °C (Ω)	26	34	55	28
R_m around T_o (Ω)	···	37	54	29

This work was supported by the DARPA MEMS/NEMS S&T Fundamentals award (Grant No. HR0011-06-1-0041) under the DARPA Center for Micro/Nano Scaling-Induced Physics (MiNaSIP).

[1] R. C. Turner, P. A. Fuierer, R. E. Newnham, and T. R. Shrout, Appl. Acoust. **41**, 299 (1994).
[2] J. A. Thiele and M. Pereira da Cunha, IEEE Trans. Ultrason. Ferroelectr. Freq. Control **52**, 545 (2005).
[3] P. M. Davulis and M. Pereira da Cunha, IEEE Trans. Ultrason. Ferroelectr. Freq. Control **57**, 59 (2010).
[4] J. R. Vig, R. L. Filler, and J. A. Kosinski, Proceedings of the 36th Annual Symposium of Frequency Control, 1982, p. 181.
[5] D. Doppalapudi, R. Mlcak, J. LeClair, P. Gwynne, J. Bridgham, S. Purchase, M. Skelton, G. Schultz, and H. Tuller, *Microelectromechanical Systems–Materials and Devices III* (Materials Research Society Symposium Proceedings, Warrendale, Pennsylvania, 2010), Vol. 1222, Paper No. 1222-DD01-02.
[6] T.-T. Yen, C.-M. Lin, X. Zhao, V. V. Felmetsger, D. G. Senesky, M. A. Hopcroft, and A. P. Pisano, Technical Digest of IEEE International Conference on Micro Electro Mechanical Systems, 2010, p. 731.
[7] T. E. Parker and M. B. Schulz, Appl. Phys. Lett. **26**, 75 (1975).
[8] J. Bjurström, G. Wingqvist, V. Yantchev, and I. Katardjiev, J. Micromech. Microeng. **17**, 651 (2007).
[9] R. Melamud, B. Kim, S. A. Chandorkar, M. A. Hopcroft, M. Agarwal, C. M. Jha, and T. W. Kenny, Appl. Phys. Lett. **90**, 244107 (2007).
[10] W. Pang, R. C. Ruby, R. Parker, P. W. Fisher, M. A. Unkrich, and J. D. Larson III, IEEE Electron Device Lett. **29**, 315 (2008).
[11] J. H. Kuypers, C.-M. Lin, G. Vigevani, and A. P. Pisano, Proceedings of IEEE International Frequency Control Symposium, 2008, p. 240.
[12] G. Wingqvist, L. Arapan, V. Yantchev, and I. Katardjiev, J. Micromech. Microeng. **19**, 035018 (2009).
[13] C.-M. Lin, T.-T. Yen, Y.-J. Lai, V. V. Felmetsger, M. A. Hopcroft, J. H. Kuypers, and A. P. Pisano, IEEE Trans. Ultrason. Ferroelectr. Freq. Control **57**, 524 (2010).
[14] F. D. Pietrantonio, M. Benetti, D. Cannatà, R. Beccherelli, and E. Verona, IEEE Trans. Ultrason. Ferroelectr. Freq. Control **57**, 1175 (2010).
[15] E. L. Adler, IEEE Trans. Ultrason. Ferroelectr. Freq. Control **36**, 223 (1989).
[16] S. Spinner and G. W. Cleek, J. Appl. Phys. **31**, 1407 (1960).
[17] B. Razavi, IEEE J. Solid-State Circuits **31**, 331 (1996).
[18] R. Farrell, V. R. Pagán, A. Kabulski, S. Kuchibhatla, J. Harman, K. R. Kasarla, L. E. Rodak, P. Famouri, J. Hensel, and D. Korakakis, *Microelectromechanical Systems–Materials and Devices* (Materials Research Society Symposium Proceedings, Warrendale, Pennsylvania, 2008), Vol. 1052, Paper No. 1052-DD06-18.